Interactive Teaching-learning Optimizer for Parameter Tuning of VSC-HVDC Systems with Offshore Wind Farm Integration

Bo Yang [1], Tao Yu [2*], Xiaoshun Zhang [2], Linni Huang [2], Hongchun Shu [1], Lin Jiang [3]

[1] Faculty of Electric Power Engineering, Kunming University of Science and Technology, 650500, Kunming, China
[2] College of Electric Power, South China University of Technology, 510640, Guangzhou, China
[3] Department of Electrical Engineering and Electronics, University of Liverpool, Liverpool L69 3GJ, United Kingdom
[*]corresponding author, Tao Yu: E-mail:taoyu1@scut.edu.cn

Abstract: This paper proposes a novel interactive teaching-learning optimizer (ITLO) for voltage source converter based high voltage direct current (VSC-HVDC) systems with offshore wind farm integration. Conventional vector control strategy is adopted, in which the parameters of eight proportional-integral (PI) loops are optimally tuned to achieve a reliable and satisfactory control performance under various operation conditions. Multiple classes are employed to realize a wider exploration compared with that of original teaching-learning based optimization (TLBO). Moreover, a small world network (SWN) is incorporated for an interactive learning among the teachers or students from different classes, such that a deeper exploitation can be resulted in. Hence, ITLO can effectively avoid a local optimum due to the appropriate trade-off between explorations and exploitations. Three case studies are carried out, such as active and reactive power tracking, short-circuit fault at power grid, and offshore wind farm connection. Simulation results verify the effectiveness and advantages of ITLO over that of existing meta-heuristic optimization algorithms.

1. Introduction

The need for more secure power grids and ever-increasing environmental concerns continue to drive the worldwide deployment of high voltage direct current (HVDC) transmission technology, which enables a more reliable and stable asynchronous interconnection of power networks that operate on different frequencies [1]. Recently, voltage source converter based high voltage direct current (VSC-HVDC) systems using insulated gate bipolar transistor (IGBT) technology have attracted enormous attentions due to the fast growing demand of inter-connection between the mainland and offshore wind farms, power flow regulation in alternating current (AC) power systems, long distance transmission, and introduction of the supergrid, which is a large-scale power grid interconnected between national power grids [2]. VSC-HVDC systems have several elegant merits, such as lower overall costs, a smaller environmental footprint, easier integration with renewable energy sources, as well as higher transmission stability and power quality compared to that of the conventional line-commutated converter based HVDC (LCC-HVDC) systems [3].

Generally speaking, a proper control system design is very crucial to guarantee the reliability and optimality of VSC-HVDC systems operation. As VSC-HVDC systems are highly nonlinear resulting from converters and also may operate in power grids with inaccurate system modelling or uncertain wind power penetrations, an enormous variety of advanced control schemes has been designed to provide a consistent and more reliable control performance, e.g., a feedback linearization control (FLC) was proposed to globally remove the system nonlinearities of VSC-HVDC systems, which however requires an accurate system model [4]. Reference [5] developed a feedback linearization based sliding-mode control (FLSMC) to provide a great robustness against system parameter uncertainties. Furthermore, a perturbation observer based sliding-mode control (POSMC) was designed in [6], which attempts to effectively handle the combinatorial effect of uncertain system parameters, unmodelled dynamics, and time-varying external disturbances with only one state measurement. Additionally, a Lyapunov function-based sliding mode control (LYPSMC) strategy was employed for a parallel AC-DC power system through an HVDC link to improve the system stability and robustness in the presence of various disturbances [7]. Moreover, literature [8] reported a perturbation observer based adaptive passive control (POAPC) for damping improvement of a multi-terminal VSC-HVDC system. However, the structure of the aforementioned approaches is relatively complicated thus they may not be easily implemented in practice.

Conventional vector control (VC) associated with proportional-integral (PI) loops has been popularly adopted in industry thanks to its promising features of easy implementation and simple structure [9]. Usually, the PI controller parameters are manually tuned based on a specific operation point of the linearized model from the original nonlinear systems via some empirical trial-and-error, which control performance might be significantly degraded as the system operation conditions often vary [10]. As a result, more reliable and efficient optimization methods are needed to optimally tune these parameters with the consideration of different operation conditions. Unfortunately, traditional gradient based algorithms may fail to obtain the optimal parameters due to their high dependence of an accurate system model, such as Newton's method [11] and interior point method [12]. As a consequence, plenty of meta-heuristic optimization approaches has been developed to handle this obstacle. A hybrid differential evolution (DE) and pattern search (PS) optimized fuzzy PI/PID controller is proposed for load frequency control (LFC) of multi-area power system in [13]. In reference [14], genetic algorithm (GA) was adopted to

optimize the location and size of distributed generation within a power distribution network considering uncertainties. Moreover, a bird mating optimizer (BMO) was designed to accurately estimate the electrical equivalent circuit parameters of photovoltaic arrays in [15]. In addition, a new particle swarm optimization (PSO) [16] algorithm was applied for combined problem of capacitor placement and network reconfiguration simultaneously in the presence of non-linear loads. Furthermore, literature [17] employed an artificial bee colony (ABO) algorithm for simultaneous optimum distributed generation placement and optimum tie-switch allocation based on maximisation of system loadability. Besides, a grouped grey wolf optimizer (GGWO) [18] was used to solve the maximum power point tracking of wind conversion systems.

The main limitation of these meta-heuristic techniques is the difficulty in determining the optimal control parameters. In particular, they may merely obtain a near optimal solution for a problem with a large number of variables, while a change in the selection of algorithm parameters would dramatically influence their effectiveness. What's worse, the challenge for the selection of these parameters can grow significantly if further hybridizations or modifications are undertaken [19]. Recently, a teaching-learning process inspired algorithm called teaching-learning based optimization (TLBO) has been proposed in [19, 20], which is based on the effect of influence of a teacher on the performance of students in a class. It has the advantages of obtaining global optimum for various continuous nonlinear functions with less computational efforts and high consistency [21]. So far, TLBO and several of its modifications have been successfully applied in various engineering applications, e.g., multi-objective optimal power flow considering the total fuel cost and total emission of the units [22]; simultaneous allocation optimization of distributed resources in radial distribution networks [23]; anticipatory load shedding for line overload alleviation [24]; optimal placement and size of distributed generation (DG) units in distribution systems [25]; and optimal reactive power dispatch (ORPD) problem for power transmission loss reduction [26], etc.

2. VSC-HVDC Modelling

The studied system is illustrated in Fig. 1, in which an offshore wind farm and a strong AC grid are connected at the PCC to transmit AC power to the rectifier. The rectifier regulates the DC voltage and reactive power, while the inverter regulates the active and reactive power, respectively. Note that the voltage of PCC us1 might vary due to the connection of offshore wind farm as the wind power is usually uncertain. In addition, only the balanced conditions are taken into account, e.g., the three phases have identical parameters and their voltages and currents have the same amplitude while each phase shifts 120° between themselves. A more detailed VSC model featuring the related switches can be employed but this would only add a slight ripple in voltage waveforms due to the associated switch action, which does not significantly affect the fundamental dynamics [28]. As a consequence, VSCs are represented by their average model [29].

The rectifier dynamics can be written at the angular frequency ω as [4, 6].

$$\begin{cases} \dfrac{\mathrm{d}i_{\mathrm{d1}}}{\mathrm{d}t} = -\dfrac{R_1}{L_1} i_{\mathrm{d1}} + \omega i_{\mathrm{q1}} + u_{\mathrm{d1}} \\ \dfrac{\mathrm{d}i_{\mathrm{q1}}}{\mathrm{d}t} = -\dfrac{R_1}{L_1} i_{\mathrm{q1}} - \omega i_{\mathrm{d1}} + u_{\mathrm{q1}} \\ \dfrac{\mathrm{d}V_{\mathrm{dc1}}}{\mathrm{d}t} = \dfrac{3u_{\mathrm{sq1}} i_{\mathrm{q1}}}{2C_1 V_{\mathrm{dc1}}} - \dfrac{i_{\mathrm{L}}}{C_1} \end{cases} \tag{1}$$

where the rectifier is connected with PCC via the equivalent resistance R_1 and inductance L_1, respectively. C_1 is the DC bus capacitor at the rectifier side, $u_{\mathrm{d1}} = \dfrac{u_{\mathrm{sd1}} - u_{\mathrm{rd}}}{L_1}$ and $u_{\mathrm{q1}} = \dfrac{u_{\mathrm{sq1}} - u_{\mathrm{rq}}}{L_1}$.

The inverter dynamics is written as

$$\begin{cases} \dfrac{\mathrm{d}i_{\mathrm{d2}}}{\mathrm{d}t} = -\dfrac{R_2}{L_2} i_{\mathrm{d2}} + \omega i_{\mathrm{q2}} + u_{\mathrm{d2}} \\ \dfrac{\mathrm{d}i_{\mathrm{q2}}}{\mathrm{d}t} = -\dfrac{R_2}{L_2} i_{\mathrm{q2}} + \omega i_{\mathrm{d2}} + u_{\mathrm{q2}} \\ \dfrac{\mathrm{d}V_{\mathrm{dc2}}}{\mathrm{d}t} = \dfrac{3u_{\mathrm{sq2}} i_{\mathrm{q2}}}{2C_2 V_{\mathrm{dc2}}} + \dfrac{i_{\mathrm{L}}}{C_2} \end{cases} \tag{2}$$

where the inverter is connected with the AC grid$_2$ via the equivalent resistance R_2 and inductance L_2, respectively. C_2 is the DC bus capacitor at the inverter side, $u_{\mathrm{d2}} = \dfrac{u_{\mathrm{sd2}} - u_{\mathrm{id}}}{L_2}$ and $u_{\mathrm{q2}} = \dfrac{u_{\mathrm{sq2}} - u_{\mathrm{iq}}}{L_2}$.

The interconnection between the rectifier and inverter through the DC cable can be represented by

$$V_{\mathrm{dc}} i_{\mathrm{L}} = V_{\mathrm{dc2}} i_{\mathrm{L}} + 2R_0 i_{\mathrm{L}}^2 \tag{3}$$

where R_0 represents the equivalent DC cable resistance. The phase-locked loop (PLL) [30] is adopted during the transformation from the abc frame to the dq frame. In the synchronous frame, u_{sd1}, u_{sd2}, u_{sq1}, and u_{sq2} are the d-, q-axis components of the PCC and AC grid$_2$ voltages; i_{d1}, i_{d2}, i_{q1} and i_{q2} are that of the line currents; u_{rd}, u_{id}, u_{rq} and u_{iq} are that of the converter input voltages. P_1, P_2, Q_1, and Q_2 are the active and reactive powers transmitted to the VSCs; V_{dc1} and V_{dc2} are the DC voltages; and i_{L} is the DC cable current.

At the rectifier side, the q-axis is set to be in phase with the PCC voltage u_{s1}. Correspondingly, the q-axis is set to be in phase of the AC grid$_2$ voltage u_{s2} at the inverter side. Hence, u_{sd1} and u_{sd2} are equal to 0 while u_{sq1} and u_{sq2} are equal to the magnitude of u_{s1} and u_{s2}, respectively. Note that this paper adopts such framework from [4-6, 8] to provide a consistent control design procedure and an easy control performance comparison, while other frameworks can also be used as shown in [9]. The only difference of these two alternatives is the representation of derived system equations, while control design is totally the same. At last, the power flows can be calculated as

$$\begin{cases} P_1 = \dfrac{3}{2}(u_{sq1}i_{q1} + u_{sd1}i_{d1}) = \dfrac{3}{2}u_{sq1}i_{q1} \\ Q_1 = \dfrac{3}{2}(u_{sq1}i_{d1} - u_{sd1}i_{q1}) = \dfrac{3}{2}u_{sq1}i_{d1} \\ P_2 = \dfrac{3}{2}(u_{sq2}i_{q2} + u_{sd2}i_{d2}) = \dfrac{3}{2}u_{sq2}i_{q2} \\ Q_2 = \dfrac{3}{2}(u_{sq2}i_{d2} - u_{sd2}i_{q2}) = \dfrac{3}{2}u_{sq2}i_{d2} \end{cases} \tag{4}$$

3. Interactive Teaching-Learning Optimizer

3.1. Principle of ITLO

Compared with TLBO, ITLO adopts multiple classes for an optimal solution searching, in which each class consists of a teacher and a group of students, as schematically shown in Fig. 2. The related concepts and principles are demonstrated as follows:

●*Teacher:* An individual owning the best solution (which has the smallest fitness function) of a class, who is responsible for teaching and guiding the students of that class to find a better solution, and also learning beneficial knowledge through interactions with other teachers.

●*Student:* An individual owning a solution with a larger fitness function than that of the teacher in the corresponding class, who endeavours to find a better solution via continuously learning the helpful knowledge from the teacher and interactions with other students.

●*Role swapping:* If a student finds a better solution than that of the teacher in one iteration, then their roles will be swapped, i.e., the promising student will be promoted as a new teacher while the incompetent teacher has to be demoted as a new student of that class in the next iteration.

3.2. Small world network

In general, the population-based algorithms, e.g., GA and PSO, are implemented for optimization with a completely deterministic or a completely stochastic interaction network. However, Watts and Strongetz [27] have discovered that the social networks in a human or animal group/society do not always strictly focus on themselves, but might often biased to some neighbourhood between themselves. Motivated by this natural phenomenon, an SWN mechanism was developed to generalize the unique feature of such social networks. It has been proved that global searching ability of the population-based techniques can be significantly enhanced with the use of SWN, e.g., PSO with SWN based dynamic topology [31] and improved SWN based group search optimization (GSO) [32]. Hence, SWN is incorporated for the interaction network construction among the teachers or students.

In the SWN, each individual can stochastically interact with any other individuals with a probability of p. Here, the probability of interaction p_{ij} between the ith individual and the jth individual can be calculated as

$$\rho_{ij} = \left(1 - \frac{k}{k_{max}}\right) \cdot C_p \tag{5}$$

where k is the iteration number; k_{max} is the maximal iteration number; C_p is the probability coefficient, with $0<C_p<1$.

3.3. Teaching between teachers and students

In general, a teacher aims to raise the average scores/grades of the entire class, such that all students can continuously improve their solutions through reducing the gap between the teacher's highest scores/grades and the relatively lower average scores/grades of the whole class, in which the solution of each student can be updated as [19, 20]

$$x_{teach}^{im} = x_k^{im} + r\left(x_k^{it} - T_F M_k^i\right) \tag{6}$$

$$x_{k+1}^{im} = \begin{cases} x_{teach}^{im}, \text{ if } f\left(x_{teach}^{im}\right) < f\left(x_k^{im}\right) \\ x_k^{im}, \quad \text{otherwise} \end{cases} \tag{7}$$

$$T_F = round\left[1 + \text{rand}(0,1)\{2-1\}\right] \tag{8}$$

$$M_k^i = \frac{1}{P_s}\sum_{m=1}^{P_s} x_k^{im} \tag{9}$$

where superscripts i and m represent the ith class and the mth student, respectively; x_k^{im} denotes the solution of the mth student in the ith class at the kth iteration; x_k^{it} is the obtained solution of the teacher in the ith class at the kth iteration; x_{teach}^{im} means the solution of the mth student learned from the teacher; M_k^i represents the average solution of the ith class at the kth iteration; f denotes the fitness function; r is a random number among the range of [0, 1]; T_F is a teaching factor determining the average solution that needs to be improved, whose value can be either 1 or 2 which is again a heuristic step and decided stochastically with an equal probability; and P_s is the population size of each class.

3.4. Interactive learning among teachers or students

Each individual (e.g., a teacher or a student) has his/her personal social (interaction) network with others. If an individual finds that others own more beneficial knowledge through interaction, then his/her current solution will be updated based on that one, which yields

$$x_{\text{learn}}^{im} = \begin{cases} x_k^{im} + r\left(x_k^{im} - x_{\text{best}}^{im}\right), & \text{if} f\left(x_k^{im}\right) < f\left(x_{\text{best}}^{im}\right) \\ x_k^{im} + r\left(x_{\text{best}}^{im} - x_k^{im}\right), & \text{otherwise} \end{cases} \tag{10}$$

$$x_{\text{best}}^{im} = \arg\min_{x_k^{jm}, j\in\Omega_k^{im}} f\left(x_k^{jm}\right) \tag{11}$$

$$x_{k+1}^{im} = \begin{cases} x_{\text{learn}}^{im}, & \text{if } f\left(x_{\text{learn}}^{im}\right) < f\left(x_k^{im}\right) \\ x_k^{im}, & \text{otherwise} \end{cases} \tag{12}$$

where x_{learn}^{im} denotes the solution of the mth individual of the ith class learned from his/her own interacted persons; x_{best}^{im} represents the best solution updated from the interacted persons at the kth iteration; and Ω_k^{im} is the set of interacted individuals of the mth person of the ith class at the kth iteration, which is determined by (5).

3.5. Comparisons of TLBO and ITLO

Each teacher only interacts with teachers from other classes via SWN, while each student can interact with students from any classes with a probability described by (5). Further, the main differences between TLBO and ITLO are highlighted in Table 1 for table of results, which can be explained as follows:

●*Range of exploration*: TLBO employs a single class of individuals for the global searching, while all the students are guided by only one teacher, hence he/she may be trapped at a local optimum as all the individuals can only gain beneficial knowledge from a single class. In contrast, ITLO raises the number of class for a wider explorations, in which each teacher can independently guide his/her own students of that class, such that the probability of finding a higher quality optimal solution can be naturally increased, that is, an enhanced global searching ability can be guaranteed.

●*Depth of exploitation*: In TLBO, each student just stochastically learns from one of the other students or a single teacher. However, the student in ITLO can learn from his/her own teacher, as well as from others through the interaction with SWN. Such interactions stem from different classes and are continuously varying according to SWN, thus a deeper exploitation can be achieved.

4. ITLO Design for Optimal PI Controller Parameters Tuning of the VSC-HVDC System

4.1. ITLO based control structure for VSC-HVDC systems

It can be observed from Fig. 3 that the VSC-HVDC control system contains two parts, i.e., the rectifier controller and inverter controller. At the rectifier side, the outer control loops regulate both the DC voltage V_{dc1} and reactive power Q_1 to obtain the dq-axes current references i_{d1}^* and i_{q1}^*, respectively, while the inner control loops regulate these two currents associated with the compensation terms $u_{\text{d1}}^{'}$ and $u_{\text{q1}}^{'}$ to obtain the final control inputs u_{d1} and u_{q1}. Similarly, at the inverter side, the outer control loops regulate both the active power P_2 and reactive power Q_2 to obtain the dq-axes current references i_{d2}^* and i_{q2}^*, respectively, while the inner control loops regulate these two currents associated with the compensation terms $u_{\text{d2}}^{'}$ and $u_{\text{q2}}^{'}$ to obtain the final control inputs u_{d2} and u_{q2}.

ITLO is adopted to optimally tune the parameters of eight PI loops. At each iteration, the controlled variables of VSC-HVDC systems will be considered into the optimization model, i.e., the fitness functions and corresponding solutions, while each solution represents a teacher or a student in ITLO. Then the solutions of all the students and teachers will be gradually improved until the final optimal parameters are found, which will be then adopted in the VSC-HVDC control systems. Three cases are taken into account, e.g., (1) active and reactive power tracking; (2) 5-cycle line-line-line-ground (LLLG) fault at PCC; and (3) offshore wind farm connection, together with the consideration of the overall control costs, the optimization model of ITLO for the studied system is constructed as (13) and (14), where the proportional gains ($K_{\text{pQ}i}, K_{\text{pVdc}}, K_{\text{pP2}}$) and integral gains

($K_{\mathrm{iQ}i}, K_{\mathrm{iVdc}}, K_{\mathrm{iP2}}$) of the outer control loops are bounded among [0, 25] and [0, 600], while in the inner control loops the proportional gains ($K_{\mathrm{pId}i}, K_{\mathrm{pIq}i}$) and integral gains ($K_{\mathrm{iId}i}, K_{\mathrm{iIq}i}$) are limited in the range of [0, 5] and [0, 250], respectively. T is the total operation time of each case. The PCC voltage and AC grid voltage u_{si} is limited between 0.2 p.u. to 1.0 p.u. and the DC voltage $V_{\mathrm{dc}i}$ ranges between 0.98 p.u. to 1.02 p.u.. Additionally, reactive power Q_{si} is bounded by -1.0 p.u. to 1.0 p.u.. Finally, the weights ω_{i1} and ω_{i2} are introduced to assign an importance credit of each control costs, which are chosen to be identically 1/4 (same importance), while the control costs are bounded by $|u_{\mathrm{q}i}| \leq$80 kV and $|u_{\mathrm{d}i}| \leq$60 kV, respectively [6].

$$\text{Minimize } f(\mathrm{x}) = \sum_{\text{Three cases}} \int_0^T \left(|Q_1 - Q_1^*| + |Q_2 - Q_2^*| + |V_{\mathrm{dc1}} - V_{\mathrm{dc1}}^*| + |P_2 - P_2^*| + \omega_{i1}|u_{\mathrm{q}i}| + \omega_{i2}|u_{\mathrm{d}i}|\right) \mathrm{d}t \quad (13)$$

$$\text{s.t} \begin{cases} K_{\mathrm{iQ}i}^{\min} < K_{\mathrm{iQ}i} < K_{\mathrm{iQ}i}^{\max} \\ K_{\mathrm{pQ}i}^{\min} < K_{\mathrm{pQ}i} < K_{\mathrm{pQ}i}^{\max} \\ K_{\mathrm{iId}i}^{\min} < K_{\mathrm{iId}i} < K_{\mathrm{iId}i}^{\max} \\ K_{\mathrm{pId}i}^{\min} < K_{\mathrm{pId}i} < K_{\mathrm{pId}i}^{\max} \\ K_{\mathrm{iIq}i}^{\min} < K_{\mathrm{iIq}i} < K_{\mathrm{iIq}i}^{\max} \\ K_{\mathrm{pIq}i}^{\min} < K_{\mathrm{pIq}i} < K_{\mathrm{pIq}i}^{\max} \\ K_{\mathrm{iVdc}}^{\min} < K_{\mathrm{iVdc}} < K_{\mathrm{iVdc}}^{\max} \\ K_{\mathrm{pVdc}}^{\min} < K_{\mathrm{pVdc}} < K_{\mathrm{pVdc}}^{\max}, i=1, 2. \\ K_{\mathrm{iP2}}^{\min} < K_{\mathrm{iP2}} < K_{\mathrm{iP2}}^{\max} \\ K_{\mathrm{pP2}}^{\min} < K_{\mathrm{pP2}} < K_{\mathrm{pP2}}^{\max} \\ V_{\mathrm{dc}i}^{\min} < V_{\mathrm{dc}i} < V_{\mathrm{dc}i}^{\max} \\ u_{si}^{\min} < u_{si} < u_{si}^{\max} \\ Q_{si}^{\min} < Q_{si} < Q_{si}^{\max} \\ u_{\mathrm{q}i}^{\min} < u_{\mathrm{q}i} < u_{\mathrm{q}i}^{\max} \\ u_{\mathrm{d}i}^{\min} < u_{\mathrm{d}i} < u_{\mathrm{d}i}^{\max} \end{cases} \quad (14)$$

Here, the number of the classes n is selected as a fixed number, which is set to be 5 for all the cases in this paper, as shown in Table 2. Besides, the initial set of individuals (students and teachers) can be obtained by randomly choosing from the feasible region, as follows:

$$x_0^{im} = (x_{\mathrm{ub}} - x_{\mathrm{lb}}) * R + x_{\mathrm{lb}}, i = 1, 2, ..., n; m = 1, 2, ..., P_s \quad (15)$$

where x_0^{im} denotes the initial solution of the mth individual in the ith class; R is a random vector, of which each element is randomly distributed among the range of [0, 1], while its size equals to the number of controllable variables; x_{ub} and x_{lb} are the upper and lower bounds of the controllable variables, respectively.

According to the obtained initial solutions by (15), the fitness function of each individual can be directly calculated by (13), then an individual with the minimal fitness function of that class will be promoted as the teacher of that class, while other individuals are degraded as the students.

Note that each teacher only interacts with teachers from other classes via SWN, i.e., a teacher will interact another teacher with a probability determined by (5).

Moreover, the mechanism of interactive learning among teachers is the same as that among students, so they are organized together through (10) to (12). Based on such interactive learning, a teacher will learn more beneficial knowledge from one of his/her interacted teachers with the minimal fitness function, thus the current solution can be considerably improved with a much smaller fitness function.

4.2. Parameter setting of ITLO

In ITLO, four parameters, the maximal iteration number $k_{\max}$, probability coefficient C_{p}, population size P_{s}, and the number of class n are very crucial thus need to be carefully selected for a desirable parameter tuning performance of VSC-HVDC systems. Here, $k_{\max}$ determines the obtained optimal solution and execution time, which is chosen from one of the integers {50, 100, 150, 200, 250} according to a proper trade-off between the execution time and the quality of the obtained optimal solution. In general, a larger $k_{\max}$ will lead to a longer execution time and a higher quality optimal solution. Through trial-and-error, it shows that the optimal solutions obtained by different algorithms remain to be constants or just changed slightly when $k_{\max} \geq$150, thus it is set to be 150 to appropriately shorten the execution time for all the algorithms. Finally, the uniform design technique [33] is adopted to find the appropriate parameters with a few experiments, which values are given in Table 2.

4.3. Overall execution of ITLO

To this end, the overall execution procedure of ITLO for VSC-HVDC systems is illustrated in Fig. 4.

5. Case Studies

The proposed ITLO has been applied for optimal PI controller parameters tuning of VSC-HVDC system, which control performance is compared to that of GA [14], GSO [34], PSO [16], and TLBO [19], respectively. The AC grids frequency is 50 Hz and the VSC-HVDC system parameters are tabulated in Table 3. Moreover, control inputs are modulated by the sinusoidal pulse width modulation (SPWM) technique [4, 6] while the switching frequency is 1620 Hz for both the rectifier and inverter [5]. The simulation is executed on Matlab/Simulink 7.10 using a personal computer with an Intel® Core™i7 CPU at 2.2 GHz and 4 GB of RAM.

Besides, ITLO and all the other algorithms are applied for offline optimization, not online optimization. In other words, when the optimal PI controller parameters are finally found, the obtained optimal PI controller parameters will be adopted and maintained thereafter. This is due to the fact that their execution time (in hour) is too long to satisfy a real-time control of VSC-HVDC systems, in which the power tacking, events happened in the connected power systems, and offshore wind farm are normally in milliseconds. The offline optimized PI controller parameters of five algorithms are written in the vector form as: GA = [175.357, 1.909, 112.931, 1.337, 271.058, 14.864, 25.692, 2.867, 344.205, 1.423, 151.927, 1.642, 153.906, 1.749, 166.499, 1.434]; GSO = [179.578, 3.864, 146.685, 2.775, 488.302, 3.676, 30.88, 1.354, 233.458, 2.255, 164.981, 2.662, 199.701, 1.238, 182.476, 2.975]; PSO = [124.26, 3.109, 130.187, 4.909, 220.369, 9.592, 28.318, 2.296, 290.554, 5.399, 131.052, 1.589, 132.892, 5.378, 147.455, 1.596]; TLBO = [201.28, 5.116, 202.18, 4.951, 501.93, 18.758, 32.971, 2.665, 398.59, 3.189, 5.075, 3.621, 202.881, 22.384, 10.597, 1.115]; ITLO = [215.56, 9.992, 208.594, 3.328, 497.461, 19.864, 36.045, 2.896, 405.675, 4.406, 156.195, 3.973, 199.967, 14.923]. Here, the element of the above vector is denoted by integral gain of reactive power Q_1 (K_{iQ1}); proportional gain of d-axis current I_{d1} (K_{pQ1}); integral gain of d-axis current I_{d1} (K_{iId1}); proportional gain of reactive power Q_1 (K_{pId1}); integral gain of DC voltage V_{dc} (K_{iVdc}); proportional gain of DC voltage V_{dc} (K_{pVdc}); integral gain of q-axis current I_{q1} (K_{iIq1}); proportional gain of q-axis current I_{q1} (K_{pIq1}); integral gain of reactive power Q_2 (K_{iQ2}); integral gain of reactive power P_2 (K_{pQ2}); proportional gain of reactive power P_2 (K_{iId2}); integral gain of q-axis current I_{q2} (K_{pId2}); proportional gain of reactive power Q_2 (K_{iP2}); proportional gain of q-axis current I_{q2} (K_{pP2}); integral gain of d-axis current I_{d2} (K_{iIq2}); respectively. Note that these parameters are the same for all of the three cases, as shown in objective function (13).

5.1. Active and reactive power tracking

Simulation results obtained under six consecutive step changes of both active power and reactive power are given in Fig. 5, which attempts to simulate sudden power variations at different operation points. It is obvious that ITLO has the smallest overshoot of active power and reactive power, together with a rapid and smooth power tracking. Moreover, it has the smallest DC voltage variation during each power tracking with the fastest convergence.

5.2. 5-cycle LLLG fault at PCC

A 5-cycle LLLG fault occurs at PCC when t=0.1s and removed at t=0.2s. Due to the fault, PCC voltage is decreased to a critical level [35, 36]. Fig. 6 illustrates that ITLO can rapidly restore the VSC-HVDC system with the smallest reactive power oscillations. In addition, ITLO can produce just a minimal AC fault current and restore it very rapidly, thus it is more effective in handling the AC fault compared to that of other algorithms. Finally, the overall control costs illustrate that ILTO just needs the least control efforts to restore the disturbed system.

5.3. Offshore wind farm connection

Due to the unpredictability and uncertainties of the wind speed [10], the injected wind power is normally a random value which may result in a voltage variation at PCC [6,8,37,38]. Hence, a sinusoidal AC voltage disturbance Δu_{s1}=19.8sin(8πt) kV (0.15 p.u.) starts at t=0.5s and ends at t=1.5s is applied to simulate the effect of offshore wind farm connection. The corresponding system responses are illustrated by Fig. 7, it clearly shows that ITLO can provide a minimal oscillation of DC voltage and reactive power, thus it is capable to effectively suppress such malignant oscillations.

5.4. Comparative studies

The integral of absolute error (IAE) indices of each approach calculated in different cases are tabulated in Table 4 for table of results. $\mathrm{IAE}_x = \int_0^T |x - x^*| \, \mathrm{d}t$ and the simulation time T=5s. Note that ITLO has a little bit higher IAE_{Q1} and IAE_{Q2} than that of TLBO, while it can obtain the optimal results in all other cases. In particular, its IAE_{Q1} is only 51.30% of that of GA in 5-cycle LLLG fault, and its IAE_{Vdc1} is merely 33.33% of that of GSO in offshore wind farm connection. The overall control costs are demonstrated in Fig. 8, which clearly shows that ITLO has the lowest overall control costs in all cases.

In addition, Table 5 provides the statistical results of fitness function obtained by different algorithms in 10 runs, in which all the performance indices of ITLO are the lowest among all algorithms. Note that all the algorithms have been executed for 10 runs, thus 10 optimal solutions with different fitness function can be obtained, among which the optimal solution with the minimal fitness function in 10 runs is regarded as the best case, while the one with the maximal fitness function is regarded as the Worst case. In particular, different runs adopt different initialization sets which are chosen according to (15). Here, the initialization sets include 3500 solutions (50 populations*5 classes*14 variables). Due to page

limits, only half of the initialization sets of the best case (25 populations*14 variables=350 solutions) are provided which can be found in Table 6.

Moreover, the smallest mean value indicates that ITLO can generally find a higher quality optimum, while the smallest relative standard deviation (Rel. Std. Dev.) verifies that ITLO has the highest convergence stability and reliability. As a result, ITLO is adequate to effectively avoid a local optimum because of a wider exploration through multiple classes, as well as a deep exploitation via SWN based interactive learning, such that a relatively high and reliable global searching ability can be guaranteed.

At last, the statistical results of execution time, convergence time, and iteration number are summarized by Table 7, in which the execution time and convergence time of GA are the shortest due to its simple structure, while that of ITLO are longer than other approaches due to its more complicated optimization mechanism resulting from the wider exploration and deeper exploitation. Note that such long execution time is acceptable in practical VSC-HVDC system operation as such optimization is in an offline manner.

It is worth noting that the solution sets of the different algorithms used for comparison are strongly depended upon the initial set of individuals. As a result, a random initialization is employed to determine the initial set of individuals by (15), instead of a simply fixed or subjective initial set. More specifically, all the algorithms use the same manner to initialize the set of individuals by (15), while their sets of initial individuals might be quite different due to the random initialization. In fact, this is also one of the main reason of executing all the algorithms in 10 runs, such that a much fair comparison of performance can be achieved instead of a merely single run with a random initialization.

6. Conclusions

A novel ITLO scheme is developed in this paper for the optimal PI controller parameters tuning of VSC-HVDC system with offshore wind farm integration. A wider exploration can be achieved by employing the multiple classes into knowledge learning, meanwhile the interactive learning among the teachers or students through SWN can provide a deeper exploitation. Under such improved optimization framework, the global searching ability of ITLO is remarkably enhanced, i.e., the local optimum can be effectively avoided. Three case studies have been undertaken to evaluate its control performance and are compared to that of other typical meta-heuristic optimization algorithms. Simulation results have verified that ITLO can smoothly track the active and reactive power reference, rapidly restore the disturbed system after a 5-cycle LLLG fault occurs at PCC, and effectively suppress the malignant oscillations of DC voltage and reactive power resulted from uncertain wind speed variations. At last, the overall control costs of ITLO are the lowest among all algorithms.

Acknowledgement

The authors gratefully acknowledge the support of National Basic Research Program of China (973 Program: 2013CB228205), National Natural Science Foundation of China (51477055, 51667010), Yunnan Provincial Talents Training Program (KKSY201604044), and Scientific Research Foundation of Yunnan Provincial Department of Education (KKJB201704007).

References

[1] Nikolas, F., Vassilios, G.A., Georgios, D.D.: 'VSC-based HVDC power transmission systems: An overview', IEEE T. Power Electr., 2009, 24 (3), pp. 592-602

[2] Hertema, D.V., Ghandhari, M.: 'Multi-terminal VSC HVDC for the European supergrid: Obstacles', Renew. Sust. Energ. Rev., 2010, 14, pp. 3156-63

[3] Asplund G.: 'HVDC grids-possibilities and challenges', 2009

[4] Rua, S.Y., Li, G.J., Peng, L. , et al.: 'A nonlinear control for enhancing HVDC light transmission system stability', Int. J. Elec. Power, 2007, 27, pp. 565-70

[5] Moharana, A., Dash, P.K.: 'Input-output linearization and robust sliding-mode controller for the VSC-HVDC transmission link', IEEE T. Power Deliver., 2010, 25(3), pp. 1952-61

[6] Yang, B., Sang, Y.Y., Shi, K., et al.: 'Design and real-time implementation of perturbation observer based sliding-mode control for VSC-HVDC systems', Control Eng. Pract., 2016, 56, pp. 13-26

[7] Dash, P.K., Nayak, N.: 'Nonlinear control of voltage source converters in AC-DC power system', ISA T., 2014, 53, pp. 1268-85

[8] Yang, B., Jiang, L., Yao, W., et al.: 'Perturbation observer based adaptive passive control for damping improvement of multi-terminal voltage source converter-based high voltage direct current systems', T. I. Meas. Control, 2016, DOI: 10.1177/0142331216641753

[9] Li, S., Haskew, T.A., Xu, L.: 'Control of HVDC light system using conventional and direct current vector control approaches', IEEE T. Power Electr., 2010, 25(12), pp. 3106-18

[10] Yang, B., Jiang, L., Wang, L., et al.: 'Nonlinear maximum power point tracking control and modal analysis of DFIG based wind turbine', Int. J. Elec. Power and Energy Sys., 2016, 74, pp. 429-36

[11] Argyros, I.K., Magrenan, A.A.: 'Extending the applicability of the local and semilocal convergence of Newton's method', Appl. Math. Comput., 2017, 292, pp. 349-55

[12] Alam, M.N., Das, B., Pant, V.: 'An interior point method based protection coordination scheme for directional overcurrent relays in meshed networks', Int. J. Elec. Power and Energy Sys., 2016, 81, pp. 153-64

[13] Sahu, R.K., Panda, S., Yegireddy, N.K.: 'A novel hybrid DEPS optimized fuzzy PI/PID controller for load frequency control of multi-area interconnected power systems', J. of Process Contr., 2014, 24, pp. 1596-608

[14] Evangelopoulos, V.A., Georgilakis, P. S.: 'Optimal distributed generation placement under uncertainties based on point estimate method embedded genetic algorithm', IET Gener. Transm. Dis., 2014, 8(3), pp. 389-400

[15] Askarzadeh, A., Coelho, L.S.: 'Determination of photovoltaic modules parameters at different operating conditions using a novel bird

mating optimizer approach', Energ. Convers. Manage., 2015, 89, pp. 608-14
[16] Sayadi, F., Esmaeili, S., Keynia. F.: 'Feeder reconfiguration and capacitor allocation in the presence of non-linear loads using new P-PSO algorithm', IET Gener. Transm. Dis., 2016, 10(10), pp. 2316-26
[17] Aman, M.M., Jasmon, G.B., Mokhlis, : 'Optimum tie switches allocation and DG placement based on maximisation of system loadability using discrete artificial bee colony algorithm', IET Gener. Transm. Dis., 2016, 10(10), pp. 2227-84
[18] Yang, B., Zhang, X. S., Yu, T., et al.: 'Grouped grey wolf optimizer for maximum power point tracking of DFIG based wind turbine', Energ. Convers. Manage., 2017, 133, pp. 427-43
[19] Rao, R.V., Savsani, V.J., Vakharia D.P.: 'Teaching–learning-based optimization: A novel method for constrained mechanical design optimization problems', Comput. Aided Design, 2011, 43, pp. 303-15
[20] Rao, R.V., Kalyankar, V.D.: 'Parameter optimization of modern machining processes using teaching–learning-based optimization algorithm', Eng. Appl. Artif. Intel., 2013, 26, pp. 524-31
[21] Chen, D.B., Zou, F., Wang, J.T., et al.: 'SAMCCTLBO: a multi-class cooperative teaching–learning-based optimization algorithm with simulated annealing', Soft Comput., 2016, 20, pp. 1921-43
[22] Haghighi, A.S., Seifi, A.R., Niknam, T.: 'A modified teaching-learning based optimization for multi-objective optimal power flow problem', Energ. Convers. Manage., 2014, 77, pp. 597-607
[23] Kanwar, N., Gupta, N., Niaz,i K.R., et al.: 'Simultaneous allocation of distributed resources using improved teaching learning based optimization', Energ. Convers. Manage., 2015, 103, pp. 387-400
[24] Arya, L.D., Koshti, A.: 'Anticipatory load shedding for line overload alleviation using teaching learning based optimization (TLBO)', Int. J. Elec. Power and Energy Sys., 2014, 63, pp. 862-77
[25] García, J.A.M., Mena, A.J.G.: 'Optimal distributed generation location and size using a modified teaching–learning based optimization algorithm', Int. J. Elec. Power and Energy Sys., 2013, 50, pp. 65-75
[26] Ghasemi, M., Taghizadeh, M., Ghavidel, S., et al.: 'Solving optimal reactive power dispatch problem using a novel teaching–learning-based optimization algorithm', Eng. Appl. Artif. Intel., 2015, 39, pp. 100-8
[27] Watts, D.J., Strogetz, S.: 'Collective dynamics of 'small-world' networks', Nature, 1999, 393, pp. 440-2
[28] Beccuti, G., Papafotiou, G., Harnefors, L.: 'Multivariable optimal control of HVDC transmission links with network parameter estimation for weak grids', IEEE T. Contr. Syst. T., 2014, 22(2), pp. 676-89
[29] Chaudhuri, N., Chaudhuri, B.: 'Adaptive droop control for effective power sharing in multi-terminal DC (MTDC) grids', IEEE T. Power Syst., 2013, 28(1), pp. 21-9
[30] Jovcic, D.: 'Phase locked loop system for FACTS', IEEE T. Power Syst., 2003, 18(3), pp. 1116-24
[31] Liu, Q., Wyk, B.J.V., Du, S., et al.: 'Dynamic small world network topology for particle swarm optimization', Int. J. Pattern Recogn., http://dx.doi.org/10.1142/S02180014166000 90 accessed 2016
[32] Yan, X., Yang, W., Shi, H.: 'A group search optimization based on improved small world and its application on neural network training in ammonia synthesis', Neurocomputing, 2012, 97(1), pp. 94-107
[33] Fang, K.T., Zhang, Y.: 'Uniform design: theory and application', Technometrics, 2000, 42(3), pp. 237-48
[34] He, S., Wu, Q.H., Saunders, J.R.: 'Group search optimizer: An optimization algorithm inspired by animal searching behaviour', IEEE T. Evolut. Comput., 2009, 13(5), pp. 973-90
[35] Jiang, L., Yao, W., Wu, Q.H., et al.: 'Delay-dependent stability for load frequency control with constant and time-varying delays', IEEE T. Power Syst., 2012, 27(2), pp. 932-41
[36] Yao, W., Jiang, L., Wen, J.Y., et al.: 'Wide-area damping controller for power system inter-area oscillations: a networked predictive control approach', IEEE T. Contr. Syst. T., 2015, 23(1), pp. 27-36
[37] Liu, J., Wen, J.Y., Yao, W., et al.: 'Solution to short-term frequency response of wind farms by using energy storage systems', IET Renew. Power Gen., 2016, 10(5), pp. 669-78
[38] Yang, B., Hu, Y.L., Huang, H.Y., et al.: 'Perturbation estimation based robust state feedback control for grid connected DFIG wind energy conversion system', Int. J. Hydrogen Energ., 2017, http://dx.doi.org/10.1016/j.ijhydene. 2017.06.222

Appendices

Table 1 The comparison between TLBO and ITLO.

Algorithm	Number of class	Interaction among individuals	Explorations	Exploitations	Global searching ability
TLBO	Single	Simple	Medium	Medium	Medium
ITLO	Multiple	Complicated	Wide	Deep	High

Table 2 The parameters used in ITLO.

Parameters	Range	Value
k_{max}	$k_{max}\geq 50$	150
C_p	$0<C_p<1$	0.9
P_s	$P_s\geq 2$	50
n	$n\geq 1$	5

Table 3 The VSC-HVDC system parameters [6].

AC system base voltage	u_{ACbase}	132kV
DC cable base voltage	V_{DCbase}	150kV
System base power	S_{base}	100MVA
AC system resistance (25km)	R_1, R_2	0.05Ω/km

AC system inductance (25km)	L_1, L_2	0.026mH/km
DC cable resistance (50km)	R_0	0.21Ω/km
DC bus capacitance	C_1, C_2	11.94μF

Table 4 IAE indices (in p.u.) of five algorithms calculated in three cases.

Cases	IAE Indices	GA	GSO	PSO	TLBO	ITLO
Power tracking	IAE_{Q1}	0.2972	0.2439	0.1838	**0.1470**	0.1624
	IAE_{Vdc1}	0.0855	0.0837	0.0842	0.0798	**0.0726**
	IAE_{Q2}	0.243	0.2698	0.1942	**0.1532**	0.1771
	IAE_{P2}	0.2219	0.2008	0.1777	0.1611	**0.1558**
5-cycle LLLG fault	IAE_{Q1}	0.0887	0.0912	0.0661	0.0558	**0.0455**
	IAE_{Vdc1}	0.0459	0.2123	0.1149	0.0470	**0.0373**
Offshore wind farm connection	IAE_{Q1}	0.0279	0.0233	0.0267	0.0195	**0.0111**
	IAE_{Vdc1}	0.0092	0.0225	0.0115	0.0081	**0.0075**

Table 5 Statistical results of fitness function (in p.u.) obtained by different algorithms in 10 runs.

Algorithm	Worst	Best	Mean	Rel. Std. Dev
GA	933.9064	4.314379	387.8964	409.3961
GSO	891.7833	3.695776	406.9689	403.6682
PSO	774.5416	3.142713	81.25954	231.0951
TLBO	3.627601	2.909602	3.31814	0.258028
ITLO	**3.143953**	**2.738256**	**2.857174**	**0.107838**

Table 6 The initialization sets of the best case.

Initial sets	K_{iQ1}	K_{pQ1}	K_{iId1}	K_{pId1}	K_{iVdc}	K_{pVdc}	K_{iIq1}	K_{pIq1}	K_{iQ2}	K_{pQ2}	K_{iId2}	K_{pId2}	K_{iP2}	K_{pP2}	K_{iIq2}	K_{pIq2}
X_1	-200	-0.10	-200	-10.95	-100	-200	-22.95	-19.46	-5	-20.93	-200	-30	-200	-10	-200	-0.10
X_2	-30	-0.13	-146.05	-0.10	-100	-109.43	-10	-12.27	-5	-25.48	-10	-0.10	-10	-7.35	-30	-0.13
X_3	-156.12	-0.10	-20	-2.76	-100	-18.88	-191.81	-8.88	-153.06	-0.10	-10	-17.35	-10	-10	-156.12	-0.10
X_4	-104.55	-3.14	-72.61	-8.35	-154.61	-37.88	-36.12	-5.51	-134.71	-1.47	-184.26	-23.98	-112.28	-3.12	-104.55	-3.14
X_5	-63.79	-9.49	-20	-0.10	-100	-30.53	-152.94	-0.10	-5	-0.10	-200	-0.10	-10	-5.60	-63.79	-9.49
X_6	-82.40	-2.62	-20	-0.10	-135.38	-9.31	-400	-11.37	-5	-0.10	-146.70	-0.10	-59.66	-1.89	-82.40	-2.62
X_7	-47.11	-0.10	-175.46	-3.99	-100	-43.13	-365.25	-0.70	-183.27	-0.10	-36.38	-0.10	-10	-0.83	-47.11	-0.10
X_8	-98.85	-10	-20	-0.10	-100	-30.51	-400	-6.53	-200	-0.10	-200	-30	-200	-10	-98.85	-10
X_9	-200	-3.46	-200	-0.10	-127.30	-186.98	-10	-0.10	-200	-0.10	-101.41	-0.10	-51.48	-1.75	-200	-3.46
X_{10}	-53.37	-0.10	-26.76	-0.10	-216.58	-139.28	-298.33	-0.10	-135.91	-17.02	-86.01	-9.25	-79.00	-0.10	-53.37	-0.10
X_{11}	-58.61	-6.70	-27.44	-0.10	-337.74	-58.88	-246.08	-1.20	-57.84	-22.02	-90.28	-0.40	-10	-2.10	-58.61	-6.70
X_{12}	-66.38	-4.97	-200	-0.10	-231.50	-32.56	-183.85	-14.55	-37.24	-0.10	-121.83	-0.10	-98.62	-10	-66.38	-4.97
X_{13}	-200	-1.68	-200	-0.10	-100	-10.87	-10	-20	-56.32	-0.10	-46.84	-28.95	-193.97	-0.10	-200	-1.68
X_{14}	-200	-3.40	-126.15	-0.56	-118.37	-30.96	-139.64	-20	-200	-0.10	-10	-0.10	-80.95	-8.71	-200	-3.40
X_{15}	-30	-0.10	-68.72	-5.20	-100	-162.03	-400	-14.49	-58.46	-16.48	-200	-7.67	-22.15	-0.10	-30	-0.10
X_{16}	-30	-6.14	-20	-0.10	-328.80	-19.48	-400	-11.78	-23.66	-28.92	-43.44	-0.10	-199.05	-8.67	-30	-6.14
X_{17}	-30	-4.65	-48.74	-1.70	-100	-51.18	-400	-1.50	-5	-30	-10	-0.10	-10	-0.10	-30	-4.65
X_{18}	-30	-9.32	-66.37	-0.10	-325.04	-48.18	-10	-10.02	-70.76	-8.57	-42.03	-7.36	-10	-0.10	-30	-9.32
X_{19}	-30	-0.10	-157.34	-4.49	-224.08	-176.70	-10	-0.10	-5	-0.10	-55.43	-0.10	-10	-3.55	-30	-0.10
X_{20}	-153.80	-10	-167.52	-7.59	-391.30	-34.37	-10	-0.10	-117.25	-4.55	-34.21	-26.46	-151.47	-10	-153.80	-10
X_{21}	-30	-0.10	-200	-0.10	-271.88	-200	-10	-0.10	-39.19	-3.29	-159.22	-9.49	-10	-0.10	-30	-0.10
X_{22}	-127.99	-2.85	-155.56	-0.62	-152.35	-55.97	-341.31	-13.96	-56.62	-12.09	-138.72	-0.22	-123.17	-2.81	-127.99	-2.85
X_{23}	-30	-5.45	-153.75	-0.10	-309.47	-106.00	-353.83	-0.10	-194.45	-8.08	-38.88	-24.20	-22.98	-9.37	-30	-5.45
X_{24}	-71.95	-2.77	-120.16	-1.42	-116.91	-28.13	-137.63	-13.56	-56.30	-8.97	-69.62	-10.70	-126.99	-0.36	-71.95	-2.77
X_{25}	-79.19	-2.43	-27.17	-0.65	-340.64	-153.92	-231.13	-16.11	-157.73	-15.06	-127.00	-23.89	-36.94	-9.30	-79.19	-2.43

Table 7 The statistical results of execution time and convergence time and iteration number obtained by different algorithm in 10 runs.

Algorithm	k_{max}	Execution time (hours)			Convergence time (hours)			Iteration number		
		Max.	Min.	Mean	Max.	Min.	Mean	Max.	Min.	Mean
GA	150	**0.1548**	**0.1459**	**0.1484**	**0.1527**	**0.0468**	**0.1286**	100	**30**	65
GSO	150	1.7088	1.6949	1.7012	1.7027	0.5437	1.4745	100	32	66
PSO	150	0.9444	0.9277	0.9382	0.6731	0.4896	0.581	61	52	56.5
TLBO	150	1.5944	1.3347	1.4347	1.4408	1.4125	1.4267	167	162	164.5
ITLO	150	16.1217	11.6997	13.9107	7.5372	7.5297	7.5335	**47**	46	**46.5**

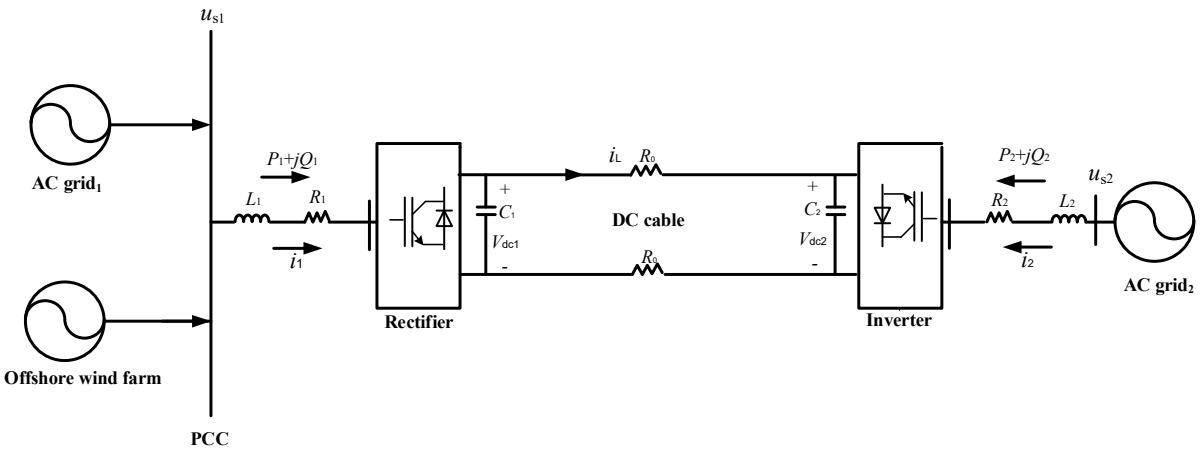

Fig. 1. *A VSC-HVDC system with an offshore wind farm integration at PCC.*

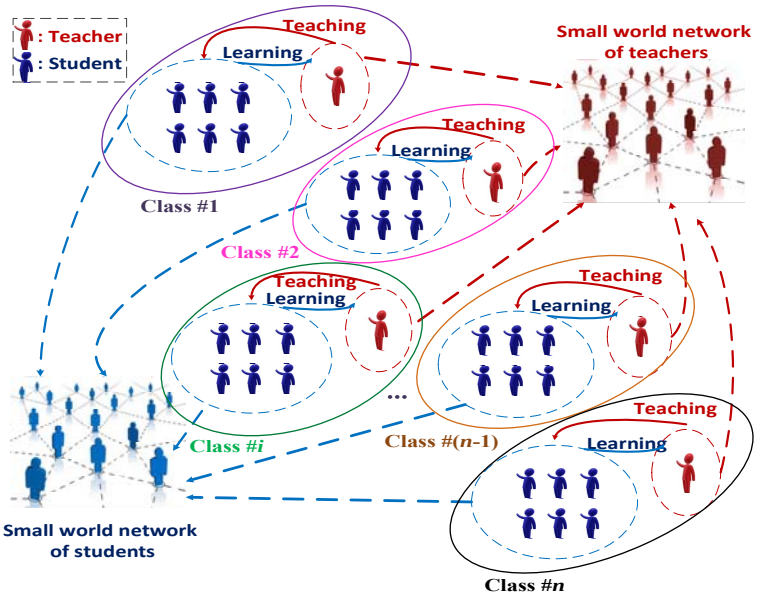

Fig. 2. *Basic optimization framework of ITLO.*

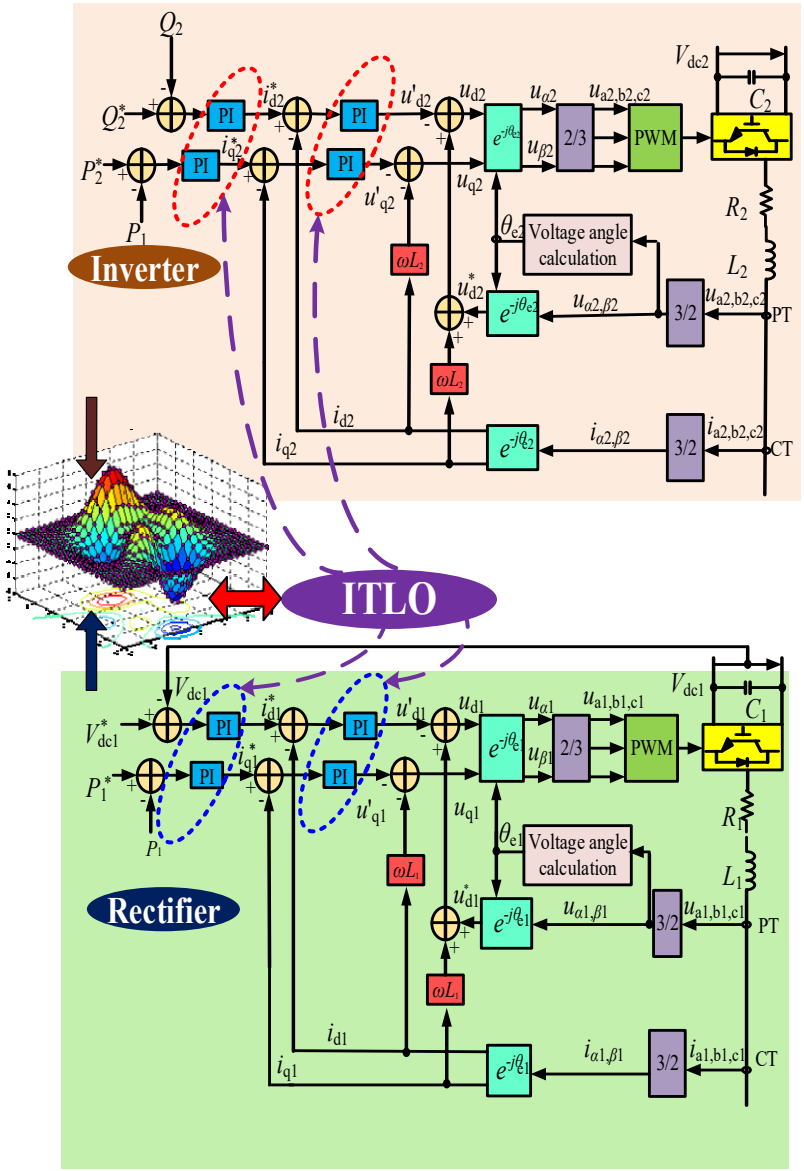

Fig. 3. *The overall ITLO based control structure of the VSC-HVDC system.*

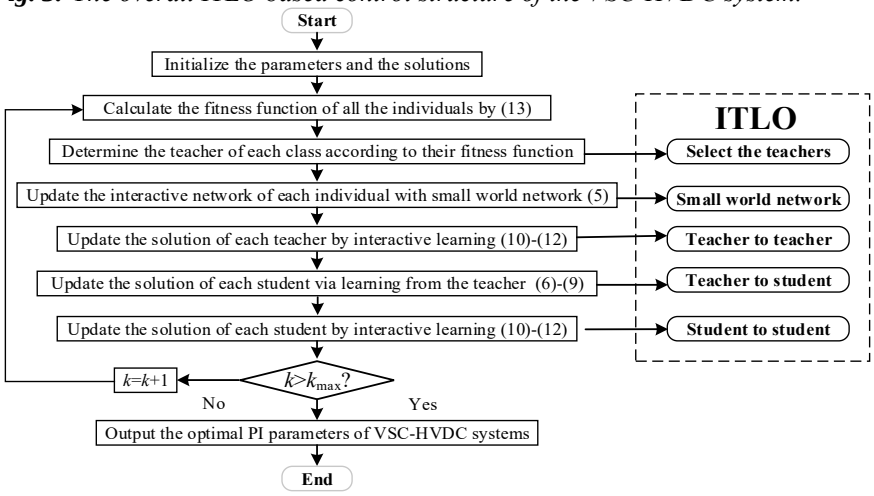

Fig. 4. *The overall execution procedure of ITLO for VSC-HVDC systems.*

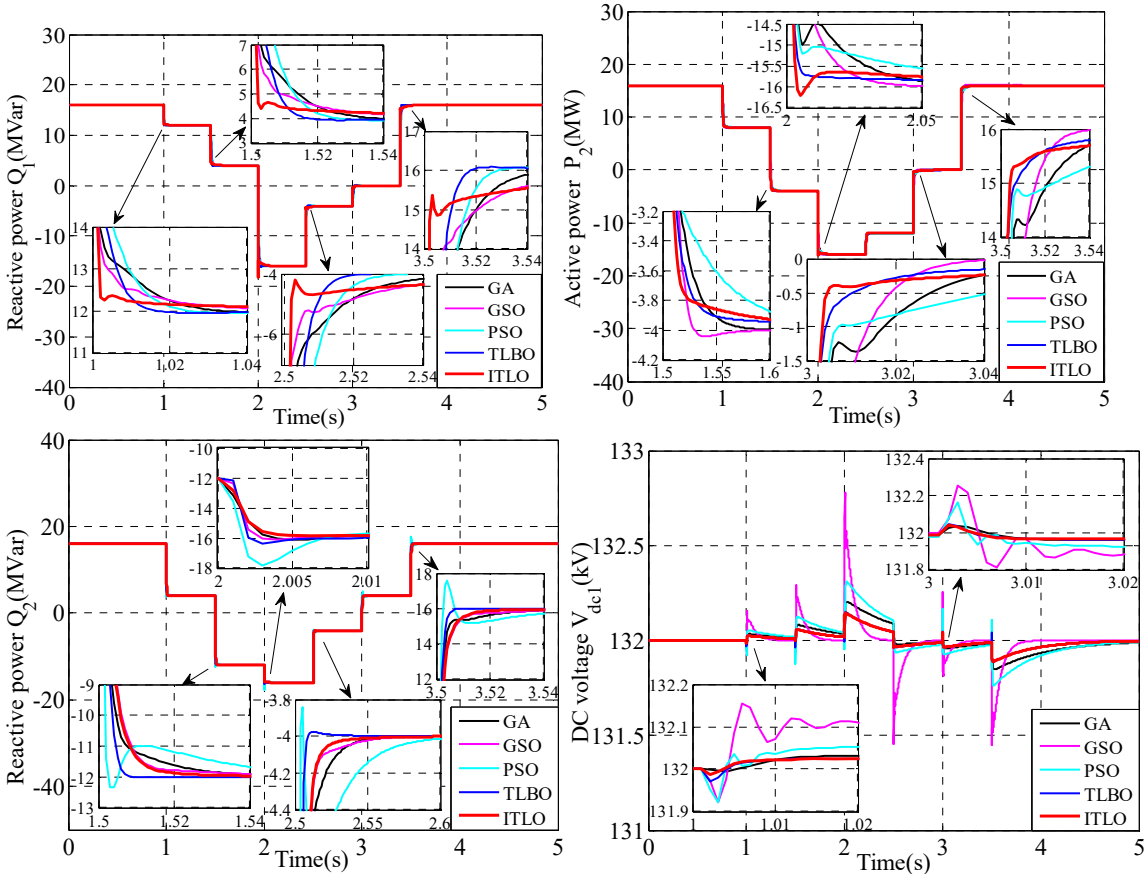

Fig. 5. *System responses obtained in active power and reactive power tracking of different algorithms.*

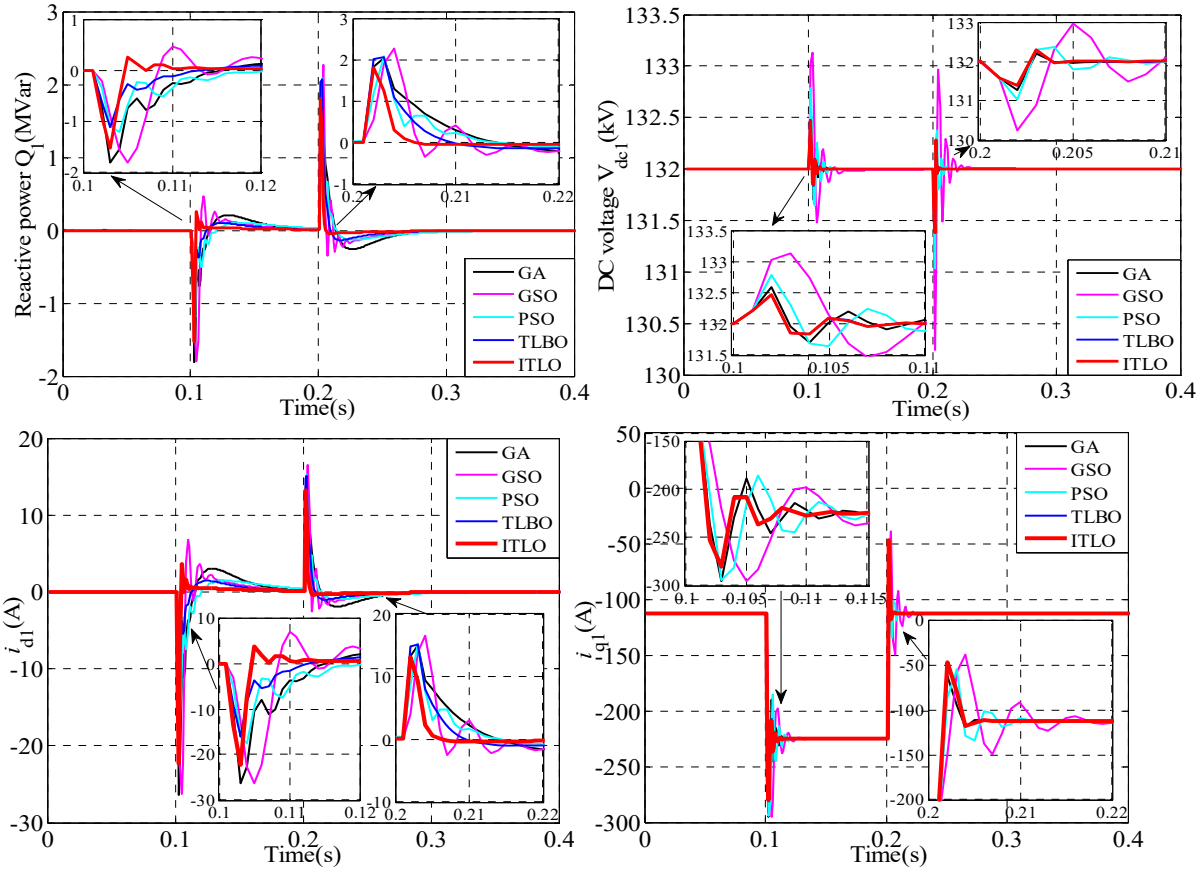

Fig. 6. *System responses obtained under a 5-cycle LLLG fault at PCC of different algorithms.*

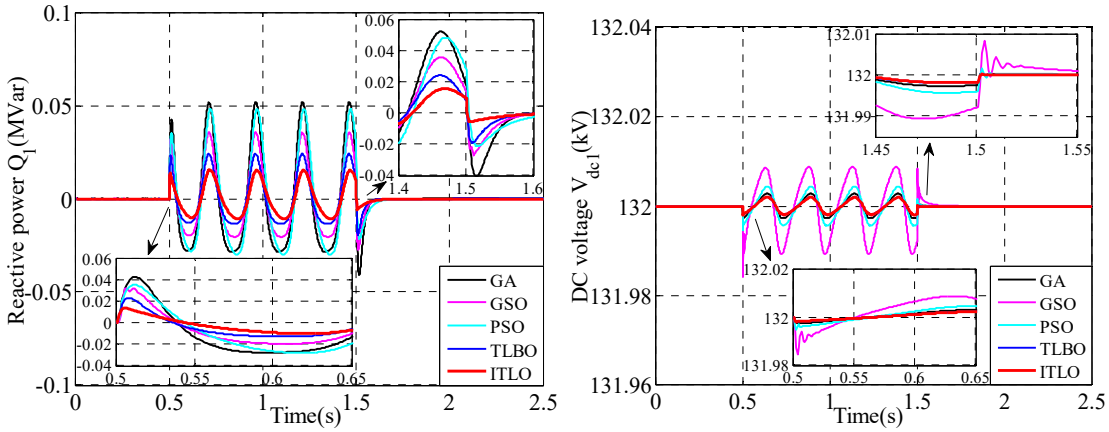

Fig. 7. *System responses of different algorithms obtained when an offshore wind farm is connected to the VSC-HVDC system.*

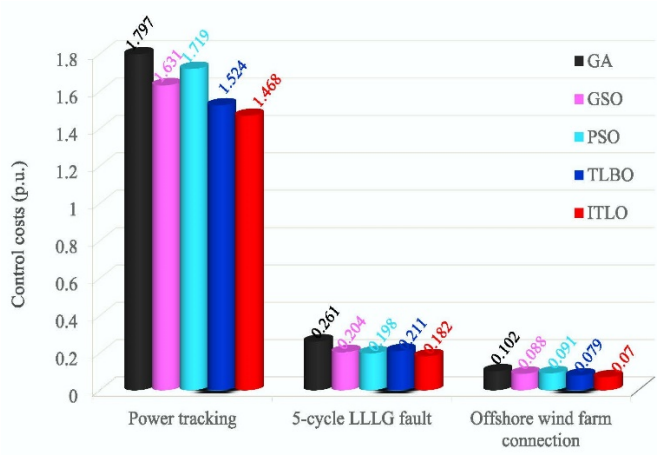

Fig. 8. *Overall control costs (in p.u.) obtained in different cases.*